Available online at www.sciencedirect.com

SciVerse ScienceDirect

Ceramics International 38 (2012) 6557–6563

CERAMICS INTERNATIONAL

www.elsevier.com/locate/ceramint

Synthesis of single-crystal SnO_2 nanowires for NO_x gas sensors application

Do Dang Trung, Nguyen Van Toan, Pham Van Tong, Nguyen Van Duy, Nguyen Duc Hoa*, Nguyen Van Hieu*

International Training Institute for Materials Science, Hanoi University of Science and Technology, No. 1 Dai Co Viet street, Hanoi, VietNam

Received 16 April 2012; received in revised form 14 May 2012; accepted 14 May 2012
Available online 31 May 2012

Abstract

Single-crystal SnO_2 nanowires (NWs) were successfully synthesized and characterized as sensing materials for long-term NO_x stability detection in environmental monitoring. Reproducible and selective growths of the SnO_2 NWs on a patterned, 5 nm-thick gold catalyst coated on a SiO_2/Si wafer as substrate were conducted by evaporating SnO powder source at 960 °C in a mixture of argon/oxygen ambient gas (Ar: 50 sccm/O_2: 0.5 sccm). The as-obtained products were characterized by field-emission scanning electron microscopy (FE-SEM), high-resolution transmission electron microscopy (HRTEM), X-ray diffraction (XRD), Raman scattering, and photoluminescence (PL). The SEM and HRTEM images revealed that the products are single-crystal SnO_2 NWs with diameter and length ranges of 70 nm–150 nm and 10 μm–100 μm, respectively. The three observed Raman peaks at 476, 633, and 774 cm^{-1} indicated the typical rutile phase, which is in agreement with the XRD results. The NWs showed stable PL with an emission peak centered at around 620 nm at room-temperature, indicating the existence of oxygen vacancies in the NW samples. The electrical properties of synthesized SnO_2 NWs sensor were also investigated and it exhibited a negative temperature coefficient of resistance in the measured range (300–525 K). The calculated activation energy E_c of SnO_2 NWs was 0.186 eV. Moreover, the SnO_2 NW sensors exhibited good response to NO_x gas. The response of the sensors to 5 ppm NO_x reached 105% at an operating temperature of 200 °C.

Keywords: Tin oxide; Nanowires; Gas sensors

1. Introduction

Air pollution caused by the emission of toxic NO_x gas, a mixture of nitric oxide and nitrogen dioxide produced by the reaction between nitrogen and oxygen gases in the air during combustion in internal engines at high temperatures, is increasing. The increase is especially evident in big cities where there is more motor vehicle traffic. NO_x gas exhaust is catalytically reduced through the reaction with NH_3 gas to reduce the amount of nitrogen oxide emissions [1]. The monitoring of exhaust NO_x gas is a key factor for effectively reducing NO_x Therefore, developing gas sensors for monitoring NO_x is necessary to reduce NO_x emissions, protect people from over-exposure to dangerous gases, and improve environmental quality.

Tin oxide is classified as an n-type semiconductor, with a band gap of 3.6 eV at room temperature, because of the oxygen vacancies in its crystal structure and its advanced physical and chemical properties. It is commonly used as a sensing material for gas sensor applications because of its high sensitivity to various gases, such as CO, C_2H_5OH, O_2, and NO_x [2]. Resistive-type sensing devices are simple and low cost, and work based on the change in the sensors' electrical resistance upon gas adsorption on the sensing material surface. SnO_2 nanowire (NW)-based sensors are highly sensitive to reduce CO, H_2, CH_4, or oxidizing gases (O_3, NO_2) because their sensing properties greatly depend on the carrier density, surface area, and the fabrication process. Gas-sensing materials with porous nanostructures show better sensitivity compared with the compacted ones [3,4]. Nanomaterials, such as nanoparticles, nanotubes,

*Corresponding authors. Tel.: +84 4 38680787; fax: +84 4 38692963.
E-mail addresses: ndhoa@itims.edu.vn (N.D. Hoa), hieu@itims.edu.vn (N.V. Hieu).

0272-8842/$36.00 © 2012 Elsevier Ltd and Techna Group S.r.l. All rights reserved.
http://dx.doi.org/10.1016/j.ceramint.2012.05.039

and NWs of SnO_2, promise relatively high sensitivity to reducing and oxidizing agents because of their high area to volume ratio. Recently, many researchers have tried to fabricate the nanostructure of SnO_2 for gas sensor applications, such as thin films [5], nanorods [6], NWs [7], and nanobelts [8]. The vapor–liquid–solid (VLS) [9], vapor–solid [10], anodic aluminum oxide, carbon nanotube template-assisted [11], and solution-based methods have been developed to synthesize metal oxide NWs [12]. The thermal evaporation method is effective for high-quality NW growth, which can enhance the stability of gas sensors. In addition, systematic investigation of the growth and gas-sensing properties of SnO_2 NWs for NO_x detection is crucial in developing NW-based gas sensors.

The current work studies the growth and physical characterizations of SnO_2 NWs synthesized using the thermal evaporation method for gas sensor applications. High quality SnO_2 NWs are easily deposited on interdigitated Pt/Ti electrodes for sensing device fabrication. The electrical and NO_x gas-sensing properties of as-synthesized SnO_2 NWs are also studied. Results revealed that the catalytic thermal evaporation method is effective for the fabrication of high quality single-crystal SnO_2 NWs for sensitive NO_x gas sensor applications.

2. Experimental

2.1. Tin oxide nanowire synthesis and characterizations

A schematic diagram of the experimental apparatus for synthesizing SnO_2 NWs is shown in Scheme 1. The apparatus successfully fabricated ZnO NWs using the method described in [13]. The synthesis system consisted of a horizontal alumina tube furnace, a quartz tube (3 cm diameter and 80 cm length) for reaction, a gas supply with attached mass flow control systems, and a rotary pump. The ends of the reaction tube were sealed with rubber O-rings. The carrier (Ar) gas-line and O_2 gas-line were connected to the left end of the quartz tube. The rotary pump was connected to the right end of the quartz tube, and a needle valve was placed between them to maintain the desired pressures. The ultimate vacuum of the set-up was approximately 10^{-2} Torr. Tin monoxide (SnO) was selected as the source material because it allows working at moderate temperature with respect to the SnO_2 powder source, and has better control of tin vapor with respect to Sn powder. Approximately 0.3 g SnO powder was charged on an alumina boat. A gold-coated, 5 nm thick, p-type (100) Si wafer was used as the substrate and placed in the same boat as the source. For investigation about the role of catalyst on the growth of NWs, the Au layer was pattered into islands of $200 \times 200\ \mu m^2$. The entire boat was covered by a quartz plate with a small opening for facilitating gas-flow into the assembly. The complete unit was placed in the horizontal quartz tube of a high-temperature furnace with a sharp temperature gradient. The temperature in the furnace was rapidly ramped up to 960 °C for 30 min. During the process, a constant pressure of 10 Torr was maintained by flowing 50 sccm Ar (99.99%) through the furnace. After a few minutes at the set-point temperature, 0.5 sccm oxygen gas was flowed through the quartz tube for 2 h. The temperature was then decreased to room temperature. The SnO_2 NWs in the white wool-like products were found on the Si substrate. The morphology and microstructures of the SnO_2 NWs were characterized by field-emission scanning electron microscopy (FE-SEM), energy dispersive spectroscopy (EDS), transmission electron microscopy (TEM), X-ray diffraction (XRD), Raman scattering, and photoluminescence (PL) spectra.

2.2. Sensor device fabrication and characterizations

As-synthesized SnO_2 NWs on the Si substrate were dispersed in a methanol solution for 5 min under ultrasonic vibration. The dispersed SnO_2 NWs were then dropped onto an interdigitated Pt/Ti electrodes fabricated on a thermally oxidized SiO_2 substrate, and were dried in air at 150 °C for 30 min. The size and the distance between the fingers of electrodes were 20 μm. The sensing device was then placed in the center of a tube furnace for heat

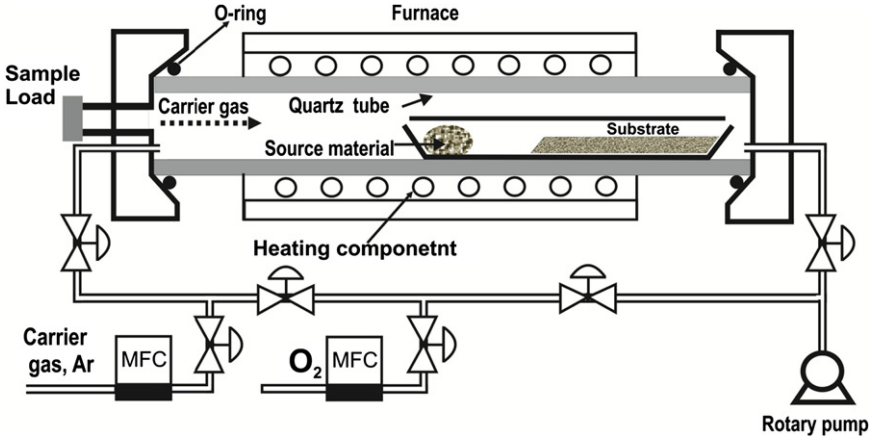

Scheme 1. The schematic diagram of tin oxide NW fabrication system. It contains a quart tube located in a horizontal furnace. The carrier gases can be introduced into the quart tube by using two mass flow controllers. Source materials and substrate were located in the center of the quart tube.

treatment process to increase the adhesion and contact between the NWs and electrodes. The heat treatment was performed in N_2 at 400 °C for 1 h. For electrical and gas-sensing property characterization, the sensors were installed in a steel stainless chamber supported by a controllable heater. The temperature of the sensor could be controlled in the range of 30 °C–400 °C. Dry air and NO_x 1000 ppm were used as carrier and target gases. Dry air and NO_x were flown through the chamber using two mass flow controllers. The flow rate could be varied to get the desired concentration of NO_x During the measurement, the total flow rate of gas was kept constant at 500 sccm to eliminate the effect of temperature shock due to the switching on/off from dried air to analytic gas. This method has been widely used in the gas sensor technology [11,13]. All the measurements were performed using a programmable Keithley 2400, which was controlled by a Labview program.

3. Results and discussion

The morphology of the as-synthesized SnO_2 NWs was characterized by FE-SEM and TEM, as shown in Fig. 1. The SnO_2 NWs only grew where the Au catalyst layer was deposited on the Si substrate, as shown in Fig. 1A. This confirmed that the SnO_2 NWs could grow only with the assistance of Au catalyst. Further investigation on the role of Au catalyst was done by the SEM image of the patterned Au layer after increasing the furnace temperature without supplying SnO for the growth of SnO_2 NWs. The SEM image reveled that during heat treatment, the Au layer was partially melted to generate the small islands of an average size of about 20 nm (Fig. 1A, inset). Those small islands acted as catalytic seeds for the growth of NWs. Therefore, the Au sphere observed on top of a NW, and the diameter of a NW were much smaller than the size of patterned Au area ($200 \times 200\ \mu m^2$). The network structures of SnO_2 NWs lay on the silicon substrate to form a porous thin film. The SnO_2 NWs had smooth surfaces with lengths reaching up to hundreds of micrometers, as shown in Fig. 1B. In the inset of Fig. 1B, the SEM image focused on the tip of a NW and confirmed the presence of the Au catalyst, indicating that the growth of NWs obeyed the VLS mechanism. The TEM image of SnO_2 NWs was also characterized and shown in Fig. 1D. The SnO_2 NWs had very smooth, single-crystal surfaces, with an average diameter of approximately 80 nm. The HRTEM image in Fig. 1D shows that the single-crystal phase of NWs had a very clear lattice structure with an interspace of 0.33 nm, which corresponded to the distance between the (110) planes of SnO_2 [11]. The single-crystal of NWs was also confirmed by the selective area electron diffraction (SAED), as shown in inset of Fig. 1D. The SAED pattern showed the bright spot diffraction of a single crystal but not the rings of polycrystals. This result is consistent with recent report on the single crystal of SnO_2 WNs fabricated by chemical vapor deposition (CVD) using Au nanoparticles as catalysts [9]. The growth mechanism of SnO_2 NWs could be explained based on the VLS mechanism first reported by Wagner and Ellis [14]. In comparison with the SnO_2 NWs synthesized in a previous work [15], the NWs in the current work did not exhibit many differences in morphology. The advantages of the synthesized method used in the current work are that the quartz tube was much less contaminated compared with that in other methods [15] and less SnO powder sources were used. In previous synthesis methods, the new quartz tube is replaced after two or three synthesis runs. The current synthesis method is convenient for growing doped SnO_2 NWs, such as Zn-, In-, and Sb-doped SnO_2 NW, which is difficult to obtain using the previous method. The doping of SnO_2 NWs is not within the scope of the current paper, and will be published in another work.

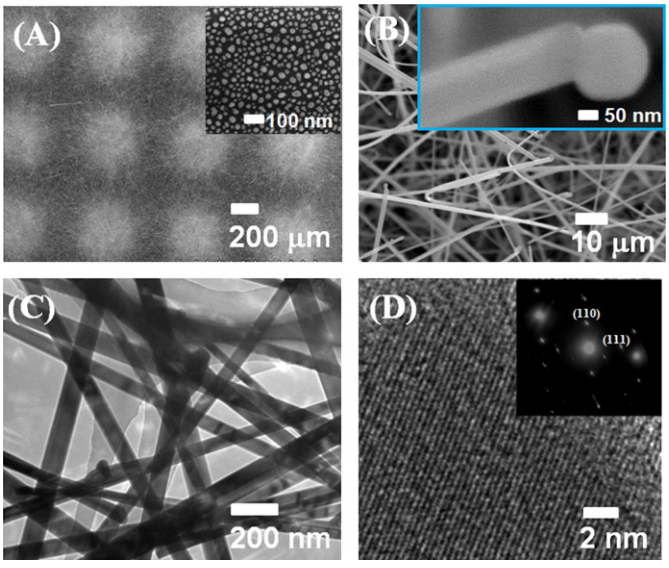

Fig. 1. (A) and (B) FE-SEM images of as-growth tin oxide NWs: insets are the SEM images of Au catalytic islands after thermal treatment ((A), inset) and the Au particle at the tip of a NW ((B), inset), respectively; (C) TEM and (D) HRTEM images of as-synthesized tin oxide NWs. Inset is SAED pattern of corresponding NW ((D), inset).

The XRD pattern of the as-obtained SnO_2 NWs is shown in Fig. 2A. All of the diffraction peaks can be perfectly indexed to the tetragonal rutile structure of SnO_2, which coincides with the reported data from the JCPDS card (77-0450). Raman characterization was also performed, as shown in Fig. 2B. Three Raman shifts (approximately 467, 633, and 774 cm^{-1}) showed that the typical feature of the rutile phase of the SnO_2 NWs coincides with previous reports [14]. Moreover, PL is a suitable technique to determine crystalline quality and the presence of impurities in the material and exciton fine structures. For these reasons, the room-temperature PL spectra of the SnO_2 NWs were characterized, as shown in Fig. 2C. It is clear that a very broad peak located at yellow emission of around 620 nm is observed for as-synthesized SnO_2 NWs. The emission peak at 620 nm (2.00 eV) is smaller than the band gap of the SnO_2 material (3.6 eV).

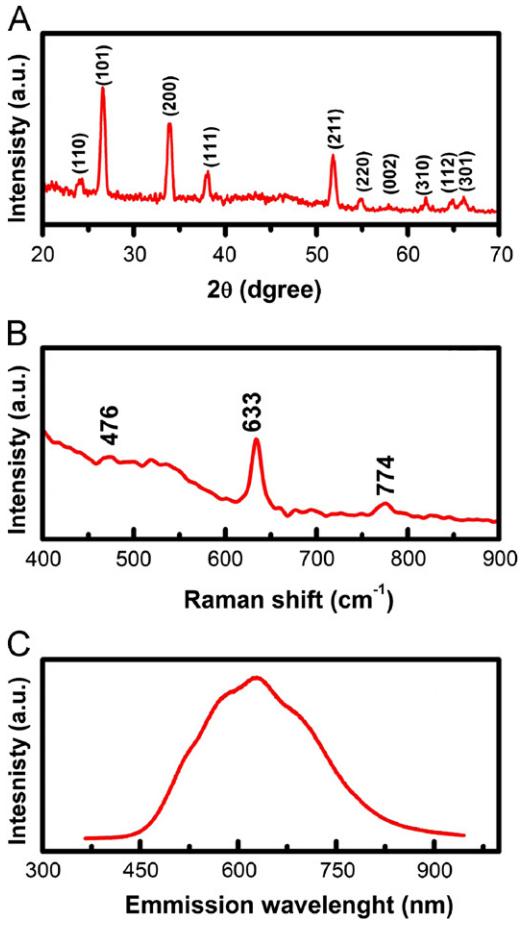

Fig. 2. Microstructure characterizations: (A) XRD pattern, (B) room-temperature Raman spectrum, and (C) room-temperature PL spectrum of as-synthesized SnO_2 NWs.

Therefore, the visible emission peaks cannot be ascribed to the direct recombination of a conduction electron in the Sn 4d band and a hole in the O 2p valence band. The semiconductor behavior of SnO_2 is attributed to the presence of oxygen vacancies, which are also crucial to their optical properties [14,15]. Therefore, the emission peak at 620 nm is believed to have originated from the luminescence centers formed by tin interstitials or the dangling bonds in the SnO_2 NWs. The oxygen vacancies with high density interact with the interfacial tin, and lead to the formation of a considerable amount of trapped states within the band gap, thus giving rise to a high PL intensity at room temperature [14–18].

The elemental analysis of as-growth tin oxide NWs by EDS is shown in Fig. 3. The EDS spectrum demonstrated the existence of Si, O, and Sn elements, in which the presence of Si was originally from the silicon substrate whereas the O and Sn were these of tin oxide NWs. The composition of tin oxide NWs estimated from the EDS analysis was about $SnO_{1.8}$. This indicated that the as-growth tin oxide NWs were un-stoichiometric due to the vacancy of oxygen in the crystal and on the surface of NWs.

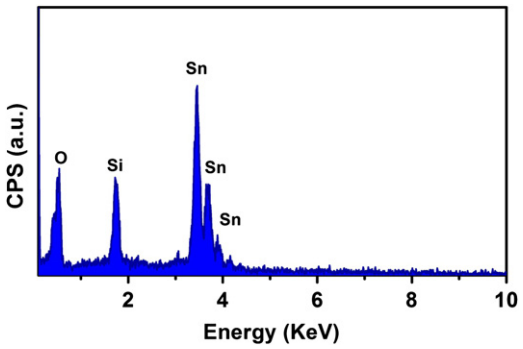

Fig. 3. EDS analysis of the as-growth tin oxide NWs sample. The presence of Si was original from silicon substrate whereas the O and Sn were from tin oxide NWs.

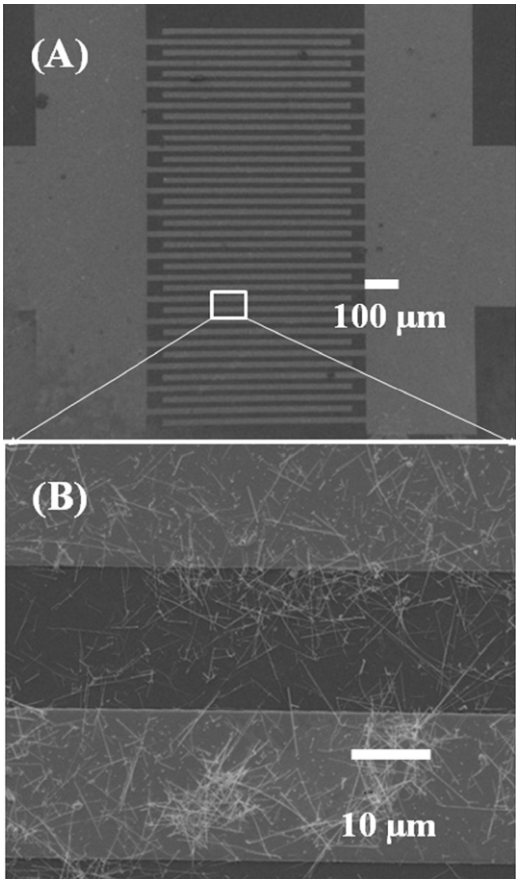

Fig. 4. SEM images of fabricated SnO_2 NWs based gas sensor: (A) the interdigitated Pt electrode deposited on a thermally oxidized silicon substrate, (B) SnO_2 NWs deposited on the silicon substrate as a network of NWs and bridging between two electrodes.

The SEM images of the gas-sensing device after fabrication are shown in Fig. 4. The deposition of SnO_2 NWs on the substrate results in the very thin layer; thus, the interdigitated Pt/Ti electrodes could be clearly seen, as shown in Fig. 4A. This occurrence ensured that all of the NWs were exposed to the analytic gas when characterized by the sensor. Fig. 4B confirms the existence of SnO_2 NWs that acted as a net of NWs to bridge the two electrodes, acting as conducting channels for current flow during

sensing measurements. In addition, when compared with the SEM image of as-synthesized NWs in Fig. 1B, it was clearly that the NWs looked shorter because the ultrasonic vibration broke them into fragments of NWs.

The dependence of the electrical resistance of sensor on temperature was measured by applying a voltage of 5 V between sensor electrodes and the current was recorded. The temperature was increased to a given value and maintained for 5 min before recording the current. The resistance was calculated by dividing the applied voltage to the recorded current; the data are shown in Fig. 5A. It is clearly that the sensor resistance decreased rapidly with increase in temperature ranging from 30 K to 525 K. Herein, the measured value involved the resistances the NWs, the contacts between individual NWs and contacts between the NWs and the metal electrodes. Therefore, the sensor resistance decreased with increasing temperature would be the results of the intrinsic semiconductor behavior of the NWs, the decrease in barrier height between individual NWs, and between the NWs and the metal electrodes. The electrical properties of the sensor are also dependent on the oxygen adsorptions on the surface of SnO_2 NWs. In ambient air, the oxygen adsorbed on the surface of SnO_2 depends on the temperature. In temperatures ranging from 300 K to 550 K, the oxygen can adsorb on the surface of the SnO_2 in the form of O_2, O_2^-, O^-, or O^{2-} [19]. The adsorbed oxygen molecules on tin oxide withdraw electrons from SnO_2 and decrease the conductivity of SnO_2. The dependence of conductivity of tin oxide semiconductor on ambient temperature is expressed by the formula [20]:

$$\sigma = \sigma_0 \exp(-E_c/(k_B T)) \quad (1)$$

where E_c is the thermal activation energy of conduction not dependent on temperature; k_B is the Boltzman constant; and T is the absolute temperature. For a more detailed investigation of the effect of temperature on the conductivity of SnO_2 NWs, the I–V curves were recorded at temperatures ranging from 300 K to 525 K in air atmosphere. The measurement results are shown in Fig. 5B. The I–V curves showed good linear behaviors, indicating an Ohmic contact between NWs and electrodes. The current increased as the temperature increased. E_c was approximately 0.186 eV, and was calculated from the fitting curve of $Ln(I)$ versus $1/T$, as shown in Fig. 5C. The activation energy E_c affected the response and recovery times of the sensor, and the smaller E_c exhibited higher sensitivity [21]. Note that the activation energy (0.186 eV) was lower compared with the optical transitions at 2 eV, and the expected bandgap of SnO_2 (3.6 eV). The lower activation energy was possibly due to the high level defect of NWs and/or the results of the contacts between NWs.

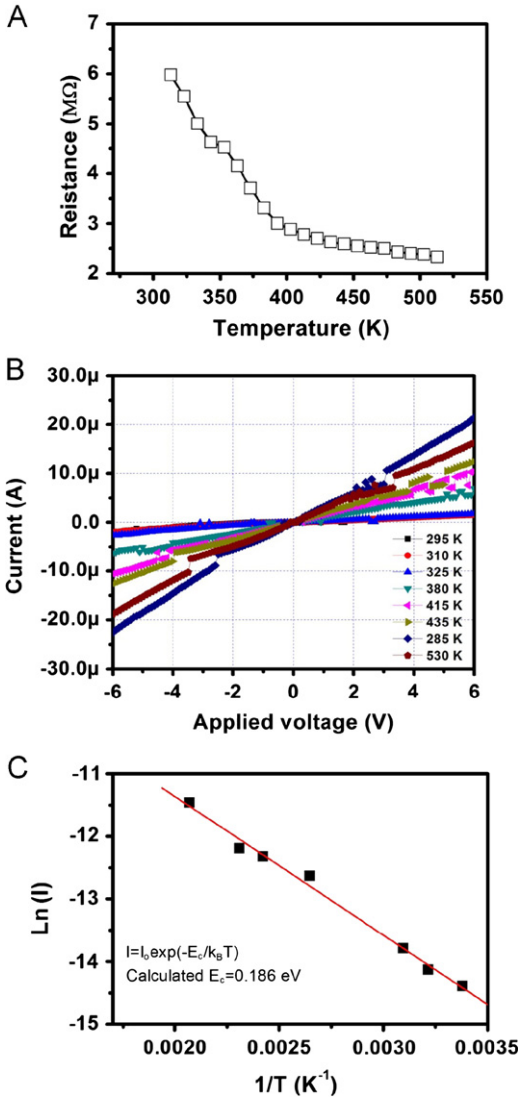

Fig. 5. Electrical characterizations of (A) the dependence of sensor's resistance on temperature; (B) the I–V curves of the sensor measured at different temperatures; and (C) $Ln(I)$ versus $(1/T)$.

NO_x is one of the most prolific toxic gases that pollute the environment. NO_x existing in the air can cause acid rain. Long-term exposure to NO_x, even at low concentrations can have adverse effects on health, such as anesthetizing the nose. The early detection of NO_x is necessary because it will help people prevent damage from the toxic gas. NO_x sensing was measured at 200 °C, the optimized working temperature of SnO_2-based sensor devices [22]. The changes in sensor resistance upon exposure to different concentrations of NO_x are shown in Fig. 6A. The resistance of the sensor increased abruptly when NO_x gas flowed into the chamber. After stopping the flow of NO_x and purging the chamber by dry air, the sensor resistance decreased rapidly to approximately the initial value. By fitting the resistance of sensors after normalization according to an exponential function, the recovery time of the sensor was about 2 min. Good recovery of the sensor was observed at an operating temperature of 200 °C, indicating that the interaction between NO_x and the surface of SnO_2 NWs is reversible. SnO_2 material is known as an n-type semiconductor with free electrons as carriers due to the vacancy of oxygen. Thus, when NO_x was adsorbed on the surface, the NO_x molecules accepted the electron from the tin oxide, decreased the carrier density, and resulted in the

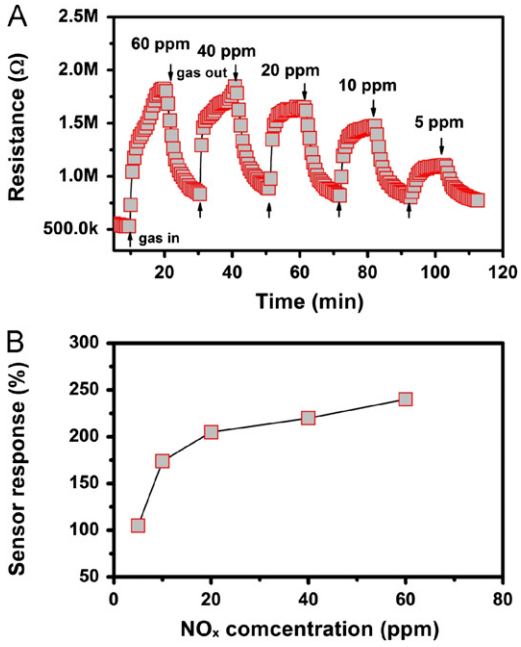

Fig. 6. (A) The change in sensor resistances upon the exposure of different concentrations of NO_x, (B) and sensor response as a function of gas concentration.

increase in sensor resistance [23,24]. The dependence of sensor response on NO_x concentration is shown in Fig. 5B. The sensor response was calculated as $S(\%)=100(R_G-R_O)/R_O$, where R_G and R_O are the sensor resistances in NO_x and dry air, respectively. The sensor response was 105% to 5 ppm of NO_x and increased as the NO_x concentration increased. This is a fairly high response value if we note that the sensitivity of SnO_2 thin film to 20 ppm NO_x measured at a similar temperature (475 K) was only 106% [25]. At concentrations higher than 20 ppm, the sensor response reached saturation values. However, this behavior did not affect the performance of the sensor when it was used to detect NO_x at low concentrations of allowable exposure limits (5 ppm) and at ppb levels.

4. Conclusion

Single-crystal SnO_2 NWs were successfully synthesized on Si substrates supported with Au thin film as catalyst by thermal evaporation method with SnO as the precursor. The high-quality, as-synthesized SnO_2 NWs, with an average diameter of 80 nm and length up to hundreds μm, have been found effective for the fabrication of NW-based gas sensors. The electrical properties of SnO_2 NWs were also studied, and found to be highly sensitive to NO_x. The SnO_2 NW-based sensor can detect the concentration of NO_x down to ppm levels with fast response and recovery.

Acknowledgments

This work was financially supported by Vietnam's National Foundation for Science and Technology Development (NAFOSTED) for a Basic Research Project (no. 103.02-2011.40) and by the National Key Research Program on Science and Technology under Contract no. 10/2011/HĐ-ĐTTN-KC02/11–15. N.V. Hieu also acknowledges to the support from Nippon Sheet Glass Foundation for Materials Science and Engineering.

References

[1] P. Forzatti, I. Nova, E. Tronconi, Enhanced NH_3 selective catalytic reduction for NO_x abatement, Angewandte Chemie 121 (2009) 8516–8518.
[2] (a) G. Eranna, B.C. Joshi, D.P. Runthala, R.P. Gupta, Oxide materials for development of integrated gas sensor-a comprehensive review, Critical Reviews in Solid State and Materials Sciences 29 (2004) 111–188;
(b) E. Comini, C. Baratto, G. Faglia, M. Ferroni, A. Vomiero, G. Sberveglieri, Quasi-one dimensional metal oxide semiconductors: Preparation, characterization and application as chemical sensors, Progress in Materials Science 54 (2009) 1–67.
[3] I. Simon, N. Barsan, M. Bauer, U. Weimar, Micromachined metal oxide gas sensors: opportunities to improve sensor performance, Sensors and Actuators B: Chemical 73 (2001) 1–26.
[4] N.D. Hoa, N.V. Quy, Y. Cho, D. Kim, Porous single-wall carbon nanotube films formed by in situ arc-discharge deposition for gas sensors application, Sensors and Actuators B: Chemical 135 (2009) 656–663.
[5] M. Epifani, L. Francioso, P. Siciliano, A. Helwig, G. Mueller, R. Díaz, J. Arbiol, J.R. Morante, SnO_2 thin films from metalorganic precursors: synthesis characterization, microelectronic processing and gas-sensing properties, Sensors and Actuators B: Chemical 124 (2007) 217–226.
[6] D. Wang, X. Chu, M. Gong, Gas-sensing properties of sensors based on single-crystalline SnO_2 nanorods prepared by a simple molten-salt method, Sensors and Actuators B: Chemical 117 (2006) 183–187.
[7] A. Kolmakov, Y. Zhang, G. Cheng, M. Moskovits, Detection of CO and O_2 using tin oxide NWs sensors, Advanced Materials 15 (2003) 997–1000.
[8] A. Kolmakov, D.O. Klenov, Y. Lilach, S. Stemmer, M. Moskovits, Enhanced gas sensing by individual SnO_2 NWs and nanobelts functionalized with Pd catalyst particles, Nano Letters 5 (2005) 667–673.
[9] (a) El-Shazly M.A. Duraia, Z.A. Mansorov, S. Tokmolden, Synthesis, characterization and photoluminescence of tin oxide nanoribbons and NWs, Physica B: Condensed Matter 404 (2009) 3952–3956;
(b) Q. Kuang, C. Lao, Z.L. Wang, Z. Xie, L. Zheng, High-sensitivity humidity sensor based on a single SnO_2 nanowire, Journal of the American Chemical Society 129 (2007) 6070–6071.
[10] S. Budak, G.X. Miao, M. Ozdemir, K.B. Chetry, A. Gupta, Growth and characterization of single crystalline tin oxide (SnO_2) NWs, Journal of Crystal Growth 291 (2006) 405–411.
[11] N.D. Hoa, N.V. Quy, H. Song, Y. Kang, Y. Cho, D. Kim, Tin oxide nanotube structures synthesized on a template of single-walled carbon nanotubes, Journal of Crystal Growth 311 (2009) 657–661.
[12] W. Wang, J. Niu, L. Ao, Large-scale synthesis of single-crystal rutile SnO_2 NWs by oxidizing SnO nanoparticles in flux, Journal of Crystal Growth 310 (2008) 351–355.
[13] N.V. Hieu, N.D. Chien, Low-temperature growth and ethanol-sensing characteristics of quasi-one-dimensional ZnO nanostructures, Physica B: Condensed Matter 403 (2008) 50–56.
[14] R.S. Wagner, W.C. Ellis, Vapor–liquid–solid mechanism of single crystal growth, Applied Physics Letters 4 (1964) 89–90.
[15] N.V. Hieu, Highly reproducible synthesis of very large-scale tin oxide nanowires used for screen-printed gas sensor, Sensors and Actuators B: Chemical 144 (2010) 425–431.

[16] W. Wang, C. XU, G. Wang, Y. Liu, C. Zheng, Synthesis and Raman scattering study of rutile SnO_2 NWs, Journal of Applied Physics 92 (2002) 2740–2742.
[17] S. Luo, P.K. Chu, W. Liu, M. Zhang, C. Lin, Origin of low-temperature photoluminescence from SnO_2 NWs fabricated by thermal evaporation and annealed in different ambients, Applied Physics Letters 88 (2006) 183112-1–183112-3.
[18] S. Luo, J. Fan, W. Liu, M. Zhang, Z. Song, C. Lin, X. Wu, P. Chu, Synthesis and low-temperature photoluminescence properties of SnO_2 NWs and nanoblets, Nanotechnology 17 (2006) 1695–1699.
[19] A. Kar, M.A. Stroscio, M. Dutta, J. Kumari, M. Meyyappan, Observation of ultraviolet emission and effect of surface states on the luminescence from tin oxide NWs, Applied Physics Letters 94 (2009) 101903-1–101903-3.
[20] H.T. Chen, S.J. Xiong, X.L. Wu, J. Zhu, J.C. Shen, P.K. Chu, Tin oxide nanoribbons with vacancy structures in luminescence-sensitive oxygen sensing, Nano Letters 9 (2009) 1926–1931.
[21] B. Ruhland, T. Becker, G. Muller, Gas-kinetic interactions of nitrous oxides with SnO_2 surfaces, Sensors and Actuators B: Chemical 50 (1998) 85–94.
[22] S.R. Morrison, The Chemical Physics of Surfaces, Plenum Press, New York, 1977.
[23] Y. Lui, W. Zhu, O.K. Tan, X. Yao, Y. Shen, Structure and gas-sensing properties of nanometer tin oxide prepared by PECVD, Journal of Materials Science: Materials in Electronics 7 (1996) 279–282.
[24] C. Canevali, C.M. Mari, M. Mattoni, F. Morazzoni, R. Ruffo, R. Scotti, U. Russo, L. Nodari, Mechanism of sensing NO in argon by nanocrystalline SnO_2: electron paramagnetic resonance, Mössbauer and electrical study, Sensors and Actuators B: Chemical 100 (2004) 228–235.
[25] I. Sayago, J. Gutiérrez, L. Arés, J.I. Robla, M.C. Horrillo, J. Getino, J. Rino, J.A. Agapito, The effect of additives in tin oxide on the sensitivity and selectivity to NO_x and CO, Sensors and Actuators B: Chemical 26 (1995) 19–23.